Global Change Biology

Global Change Biology (2012) **18**, 2041–2056, doi: 10.1111/j.1365-2486.2012.02649.x

Spatial patterns and drivers of fire occurrence and its future trend under climate change in a boreal forest of Northeast China

ZHIHUA LIU*, JIAN YANG*, YU CHANG*, PETER J. WEISBERG† and HONG S. HE*‡

*State Key Laboratory of Forest and Soil Ecology, Institute of Applied Ecology, Chinese Academy of Sciences, Shenyang, 110164, China, †Department of Natural Resources and Environmental Science, University of Nevada-Reno, 1664 N. Virginia Street, M.S. 186, Reno, NV 89557, USA, ‡School of Natural Resources, University of Missouri, 203 ABNR Building, Columbia, MO 65211, USA

Abstract

Understanding the spatial patterns of fire occurrence and its response to climate change is vital to fire risk mitigation and vegetation management. Focusing on boreal forests in Northeast China, we used spatial point pattern analysis to model fire occurrence reported from 1965 to 2009. Our objectives were to quantitate the relative importance of biotic, abiotic, and human influences on patterns of fire occurrence and to map the spatial distribution of fire occurrence density (number of fires occurring over a given area and time period) under current and future climate conditions. Our results showed human-caused fires were strongly related to human activities (e.g. landscape accessibility), including proximity to settlements and roads. In contrast, fuel moisture and vegetation type were the most important controlling factors on the spatial pattern of lightning fires. Both current and future projected spatial distributions of the overall (human- + lightning-caused) fire occurrence density were strongly clustered along linear components of human infrastructure. Our results demonstrated that the predicted change in overall fire occurrence density is positively related to the degree of temperature and precipitation change, although the spatial pattern of change is expected to vary spatially according to proximity to human ignition sources, and in a manner inconsistent with predicted climate change. Compared to the current overall fire occurrence density (median value: 0.36 fires per 1000 km^2 per year), the overall fire occurrence density is projected to increase by 30% under the CGCM3 B1 scenario and by 230% under HadCM3 A2 scenario in 2081–2100, respectively. Our results suggest that climate change effects may not outweigh the effects of human influence on overall fire occurrence over the next century in this cultural landscape. Accurate forecasts of future fire-climate relationships should account for anthropogenic influences on fire ignition density, such as roads and proximity to settlements.

Keywords: boreal forest, climate change, fire, Northeast China, spatial point pattern analysis

Received 7 December 2011 and accepted 13 January 2012

Introduction

The heterogeneous distribution and density of fire occurrence (the origin of the fire) can be predicted by a suite of biotic, abiotic, and human controls (Parisien & Moritz, 2009). Such controls may vary over space and time in their influence on forest fires and are pertinent for projecting fire activities under a changing environment. However, the predictions of fire response to climate change often assume a strong climate-fire linkage with relatively less emphasis on other controls (Flannigan *et al.*, 2009a; Wotton *et al.*, 2010), possibly due to the tight coupling between historical fire occurrence and climate that has been frequently reported (Westerling *et al.*, 2006; Marlon *et al.*, 2008; Daniau *et al.*, 2010). However, such climatic effects may be altered in strongly human-dominated landscapes, where effects of climate change on fire regime may be amplified, weakened or otherwise altered in surprising ways. To gain a thorough understanding of the spatial distribution of wildfire patterns in a climate change context, the relationship among fire and controlling factors needs to be carefully examined, especially in human affected landscapes.

Fire patterns are influenced by the distribution of environmental resources (fuels), favorable environmental conditions (topography, climate, and day-to-day weather conditions), and ignition agents (Cary *et al.*, 2006; Parisien & Moritz, 2009). Fuels provide the raw material acted on by fire. Variations in climate regulate fire occurrence patterns by affecting fuel availability through vegetation productivity (Nemani *et al.*, 2003; Zhao & Running, 2010) and the probability of lightning

Correspondence: Jian Yang, tel. + 86 24 8397 0331, fax + 86 24 8397 0300, e-mail: yangjian@iae.ac.cn

ignition (Williams, 2005). Climate gradients can also influence fire occurrence, with drier environments in otherwise mesic biomes typically displaying greater fire activity than wetter ones (Mitchener & Parker, 2005). Elevation influences fire occurrence directly through affecting lightning density (Dissing & Verbyla, 2003), and indirectly by contributing to shifts in fuel and moisture content via changing temperature and water availability (Lafon & Grissino-Mayer, 2007). Aspect affects fuel moisture content due to variation in insolation (Rollins *et al*., 2002). Humans can have both positive and negative effects on fire. Higher human population density often increases ignition sources, whereas fire prevention activities tend to decrease fire occurrence; hence fire occurrences tend to be highest at intermediate population densities (Syphard *et al*., 2007; Yang *et al*., 2008). Spatial patterns of fire occurrence over landscape scales result from the interactions among top-down controls such as climate and bottom-up controls such as local fuel conditions, weather and topography (Falk *et al*., 2011). Active fire management requires a firm understanding of the biophysical and human controls underlying wildfire patterns and of the distribution of fire occurrence hotspots. Therefore, quantitating the empirical relationship among these controls and the spatial patterns of wildfires is critical for predictive modeling of future fire regimes and fire risk.

Climate controls fuel availability and fuel moisture content, and therefore climatic change is expected to profoundly impact wildfire occurrence. The influence of climate change on fire may become more dramatic in boreal forests, where fire climate is more limiting than fuels for influencing fire frequency, severity and size (Bessie & Johnson, 1995; Fauria & Johnson, 2006; Flannigan *et al*., 2009b). Many studies have used historical data to predict the response of future fire occurrence to climate change (Flannigan *et al*., 2009b). Several studies have developed regression models predicting historical fire occurrence as a function of climate indices; when such models are extrapolated to future climate conditions, dramatic increases in fire occurrence are predicted by the end of the 21st century (Wotton *et al*., 2003, 2010; Girardin & Mudelsee, 2008; Krawchuk *et al*., 2009a). These studies, however, are usually conducted at very coarse spatial resolution (>100 km^2), limiting their potential applications to fire and fuel management at landscape and regional scales. Therefore, spatially explicit analysis of fire occurrence patterns with respect to various controls at fine scale is required to accurate prediction of fire response to climate change.

Boreal forests in Northeast China store 1.0–1.5 Pg C and contribute to approximately 24–31% of the total carbon storage in China (Fang *et al*., 2001). This region is also fire prone, with an estimated historical mean fire return interval of 30–120 years (Xu, 1998). However, recent global analysis on fire response to climate showed a great deal of uncertainty in boreal forests of Northeast China (Scholze *et al*., 2006; Krawchuk *et al*., 2009b; Pechony & Shindell, 2010). For example, Krawchuk *et al*. (2009b) constructed statistical models of the relationship between fire activity and various environmental controls at a spatial resolution of 100 km, and predicted that fire in this region would decrease. On the contrary, Pechony & Shindell (2010) combined global fire and climate modeling approaches at a spatial resolution of half degree, and projected an increased trend of fire in this region. This discrepancy implies that the aforementioned global-scale studies may not satisfactorily capture fine scale variation of fire-climate interactions. In addition, human activities play an important role in fire occurrence, but are not sufficiently incorporated in these studies. In boreal forests, vegetation dynamics and carbon balance are especially sensitive to alterations in fire regime (Scholze *et al*., 2006; Bond-Lamberty *et al*., 2007; Johnstone *et al*., 2010), making it essential to develop reliable forecasts of changes in fire activity at finer spatial scales.

The primary objectives of this study were to quantitate the relationship among fire occurrence and a suite of abiotic, biotic, and anthropogenic factors, and to model the spatial distribution of fire occurrence under current and future climate conditions in a boreal forest landscape of the Great Xing'an Mountains in Northeast China. Spatial point pattern (SPP) analysis was used to predict fire occurrence density over fine spatial scales to address the following questions: (i) What are the marginal effects of spatial control on fire occurrence pattern? (ii) What are the key spatial controls that influence the fire occurrence pattern? (iii) How is the future distribution of fire occurrence density likely to respond to predicted climate change?

Materials and methods

Study area description

Our study area located on the northern and eastern slope of the Great Xing'an Mountains (from 50°10′ N–53°33′ N and 121°12′ E–127°00′ E) in Northeast China, and encompassed approximately 8.46×10^4 km^2. The area has a cold, continental climate, with average annual temperature declining from 1 °C at its southern extremes to −6 °C at its northern extremes, and precipitation declining from 442 mm in the south to 240 mm in the north. More than 60% of the annual precipitation falls in the summer season from June to August (Zhou, 1991). The vegetation of this area is representative of cool temperate coniferous forests, forming the southern extension of the eastern Siberian boreal forests. The overstory

species include larch (*Larix gmelini*), pine (*Pinus sylvestris* var. *mongolica*), spruce (*Picea koraiensis*), birch (*Betula platyphylla*), two species of aspen (*Populus davidiana, Populus suaveolens*), willow (*Chosenia arbutifolia*), and a shrub species *Pinus pumila*. Boreal conifer tree species (mainly larch) are late successional and widely distributed, occupying moist and cooler sites. Broadleaf tree species (e.g. birch and aspen) are early successional and occupy drier, well-drained sites (Xu, 1998). Historically, fires were ignited primarily by lightning (Xu *et al*., 1997). Dendrochronological studies have indicated that the historical fire regime was characterized by frequent, low-intensity surface fires mixed with infrequent stand-replacing fires in this eastern Siberian boreal forest, with fire return interval ranged from 30 to 120 years (Xu *et al*., 1997). However, forest harvesting and fire suppression have altered fire regimes in this region (Li *et al*., 2006; Chang *et al*., 2007). Currently, fires have been infrequent, but more intense; with a fire return interval of more than 500 years (Chang *et al*., 2007).

Overall study design

We divided the fire occurrence data set into human- and lightning-caused fires, and analyzed them separately. Reported fire ignition (origin) locations for each category and relevant spatial covariates were mapped and processed using a GIS. To address research question 1, we performed exploratory analyses on the marginal effects of spatial covariates on the fire occurrence pattern. For categorical variables, we graphically compared the expected and observed fire frequency on each variable class to identify which variable class is more susceptible to fire. For continuous covariates, we used a lurking variable plot technique (Baddeley *et al*., 2005) to quantitate the variable ranges that are more susceptible to fires than others. To address research question 2, we compared the change in Akaike information criterion (ΔAIC) values between a full Poisson point process (PPP) model and the models with the removal of each individual covariate. The higher ΔAIC value is, the more important the corresponding covariate is on controlling fire pattern. To address research question 3, we selected a parsimonious inhomogeneous PPP model to fit the fire occurrence data. Then, the parsimonious PPP model was applied to map the current spatial distribution of fire occurrence density. Parameters estimated from the parsimonious model were also applied to future climate data to generate projections of the spatial distribution of fire occurrence density for 2100. We calculated the spatial change of fire occurrence density between current and future climate to highlight the response of fire occurrence to climate change. Finally, we combined the spatial change of human- and lightning-caused fire occurrence density to evaluate the overall (human- + lightning-caused) fire response of climate change.

Spatial data

Dependent variables: fire atlases. The fire dataset for Great Xing'an Mountains included the following information for all reported fires for the 45-year period from 1965 to 2009: fire origin location, size, date of occurrence, vegetation type, and ignition cause. A total of 1378 fires, which burned 6.64 million hectares, were identified based on the dataset. Lightning-caused fires constituted 43% of total fires and accounted for 5.6% of total burned area. Human-caused fires (such as arson, cooking fire, smoking, railway, and power line) constituted 21% of total fires and accounted for 66.5% of the total burned area. Fires of unknown origin constituted 36% of total fires and accounted for 27.9% of the total burned area. However, fires of unknown origin were likely caused by human activities (Personal communication with local forest managers), and also because they were mainly clustered near the human factors. In this study, we separately analyzed human-caused fires, which includes both human-caused and unknown origin fires, and results in a total of 782 fires, and lightning-caused fires, which results in a total of 596 fires (Fig. 1). Most of human-caused fires occurred in the spring (25.7, 32.6, and 22.3% in April, May, and June), whereas most of lightning fires occurred in the spring and summer (18.9, 52.6, 11.4, and 13.1% in May, June, July, and August). The annual dynamics for human- and lightning-caused fires can be found in Appendix A1 (Supporting Information).

Explanatory variables: topography, vegetation type, climate, and human factors. A 90-m resolution grid of digital elevation model (DEM) data was generated from contour lines downloaded from the National Geomatics Center of China. Slope and aspect surfaces were derived from the DEMs. Aspect was reclassified into mesic for low-potential solar insolation (NE, NW, N, and E) and xeric for high-potential solar insolation (SW, SE, S, and W) in areas with slope >0; and flat in areas with slope = 0. To examine the effects of slope positions and landform category on fire occurrence, we further classify the landscape into bottomland, flat slope, steep slope, and ridge top based on Jenness (2005).

A vegetation cover map was derived from the Vegetation Map of the People's Republic of China (VMPRC, 1 : 1 000 000; Hou *et al*., 1982), which was originally produced in 1982 and digitized in 2007 (Editorial Committee of Vegetation Map of China, 2007). Vegetation types were grouped into four categories: coniferous forest (53.4% of the total area), mixed forest (4.1%), broadleaf forest (12.6%), and meadow and others – e.g. shrub and wetland – (29.4%). Because meadow constituted most of the area for meadow and others, therefore we will refer to this vegetation type as meadows hereafter. The aggregated vegetation type map was interpolated to yield a resolution of 90-m grid cells. We assumed the aggregated vegetation types to be relatively unchanged over the study period, although forest age structure or composition may have been greatly altered by disturbances such as timber harvesting.

Annual temperature and precipitation were selected as climate factors because they influence fire occurrence by constraining fuel moisture content, and also are traditional' indicators for the degree of climate change (Scholze *et al*., 2006). Mean annual temperature and precipitation for 1965–2005 have been generated from 88 weather stations across Northeast China (Liu *et al*., 2011). Climate data were interpolated into ArcGIS grids at 1-km resolution using kriging

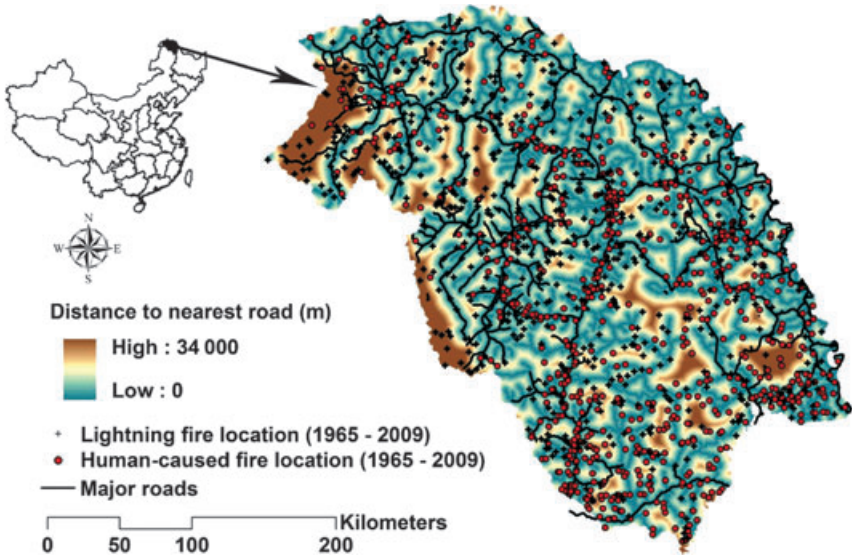

Fig. 1 Study area with reported human-caused (red circle) and lightning (black cross) fire locations (1965–2009), roadway coverage, and proximity to roads.

algorithms, resulting in continuous maps of current mean annual temperature and precipitation for Northeast China.

Fuel moisture conditions have been found to be useful predictors of fire occurrence in boreal forests (Wotton *et al.*, 2010). We selected Fine Fuel Moisture Code (FFMC) and Duff Moisture Code (DMC), which are components of the Canadian forest fire weather index, as the indicators of fuel moisture contents. FFMC tracks the moisture contents of surface litter, and is an important influence on the duration and intensity of surface fire spread. DMC describes the upper portion of organic layer in the forest floor, and strongly influences the longevity of smoldering combustion. Higher FFMC and DMC values indicate drier surface fuels, and therefore suggest a higher fire potential. FFMC and DMC were determined by daily observation of temperature, precipitation, relative humidity, and wind speed and were calculated according to Van Wagner (1987). Daily meteorological data were obtained from NECP reanalysis data (http://www.esrl.noaa.gov/psd/, accessed 7 October 2011) for periods from 1981 to 2000. The NECP reanalysis data have a spatial resolution of 1.875 degree × 1.92 degree. We selected 10 grid cells, which fall within and around our study area. We calculated the daily FFMC and DMC for fire season (March 10 to November 20) for the 20 years for each grid cell (n = 2 codes × 264 days × 20 years × 10 grid cells). We used 90th percentile levels of FFMC and DMC for each grid cells to represent fuel moisture content conditions, because previous study has proved that the tails of these moisture code distributions tends to be more relevant to true levels of fire potential as the majority of fire activity occurs on these drier days (Flannigan & Wotton, 2001). The two daily fuel moisture codes were interpolated at a resolution of 1-km across the study region using cokriging with elevation as a covariate. Therefore, we used average daily fuel moisture over 20 years, and quantified the effects of spatial variation of fuel moisture, rather than its temporal variation, on distribution of fire occurrence density.

Human infrastructure, such as roads and settlements, influences fire occurrence probability by determining accessibility of human ignition sources to forests and amount of human presence. A digital roadway coverage (scale of 1 : 100 000) was obtained from the National Geomatics Center of China. Given that most roads were built prior to 1990, we assumed that the road network had remained constant over the study period. Proximity to roads and settlements was calculated as the Euclidean distance from each cell to the nearest road (Fig. 1) or settlement. Road density (i.e. length of road within each square kilometer) was derived via use of a moving window analysis.

Lightning data were downloaded from the NASA Global Hydrology and Climate Centre Lightning Team's high resolution annual lightning climatology data set (Christian *et al.*, 2003). The lightning data reported global mean annual flash rates per km^2 from data collected between 1995 and 2005, and was stored on a half-degree hierarchical data format. A lightning density map for our study area was subset from the global lightning density map, and then was interpolated to a1-km resolution map using cokriging with elevation as covariate.

Climate change data. Climate change data were obtained for the 2081–2100 time period (hereafter: 2100) from the output of two well-established General Circulation Models (GCMs): UK Hadley Center for Climate Prediction and Research (HadCM3) and the Canadian Centre for Climate Modeling and Analysis (CCCma) Coupled Global Climate Model (CGCM3). These two GCMs have been widely applied to Northeast China (Zhou, 2007; Bu *et al.*, 2008; Liu *et al.*, 2011), and were considered to well capture the current and future climate condition in the region. For each GCM, we used projected annual

temperature and precipitation data from two (B1 and A2) Special Report on Emissions Scenarios to represent future climate conditions, for a total of four climate change scenarios. Although they may be criticized for not capturing the lower and upper limits of greenhouse gas concentrations than expected, the B1 and A2 scenarios are widely used to represent the greatest divergences in scenarios depicting future greenhouse gas concentrations (i.e. 550–720 ppm) (Nakicenovic *et al*., 2000). Future climate predictions were calibrated using historical data (Appendix A2). We first calculated the annual temperature and precipitation bias between simulated and recorded historical data from 1965 to 2000, using the 20C3M scenario. If the climate bias was positive (i.e. predicted annual temperature and precipitation was greater than the historical data during the 1965–2000 period), then the difference was subtracted from the predicted annual values. Otherwise, the difference was added to the predicted annual values. We downloaded the projected historical' (HadCM3-20C3M, CGCM3-20C3M) and future climate data (HadCM3-A2, HadCM3-B1, CGCM3-A2, and CGCM3-B1), which had a downscaled resolution of 0.085° (10 km) for China, at Data Sharing Infrastructure of Earth System Science of China (http://www.geodata.cn/, accessed 17 June 2011). The average annual temperature and precipitation for 2100 were interpolated to a 1-km resolution grid format so that spatial resolutions of all spatial covariates are consistent in the modeling.

To calculate fuel moisture conditions (FFMC and DMC) under future climate scenarios, we used daily meteorological data predicted for 2081–2100. We first calculated the average monthly delta values of temperature, precipitation, relative humidity, and wind speed between projected historical' (1981–2000) climate (HadCM3-20C3M, CGCM3-20C3M) and the future (2081–2100) climate (HadCM3-A2, HadCM3-B1, CGCM3-A2, and CGCM3-B1) for each projected grid cell covered our study area. We then added the average monthly delta value to the current daily NCEP reanalysis data for the corresponding calendar month, to derive daily meteorological data predicted for 2081–2100. As GCM output has a different spatial resolution than the NCEP reanalysis data, the delta value for each GCM cell was added to the nearest centroid of NCEP reanalysis grid cells. The GCM monthly data were downloaded from World Climate Research Programme's (WCRP) phase III of the Coupled Model Intercomparison Project (CMIP3; http://esg.llnl.gov:8080/index.jsp, accessed 7 October 2011). To be consistent with the current fuel moisture conditions, 90th percentile levels of future FFMC and DMC were used to represent fuel moisture content during 2081 and 2100 for each grid cells, after interpolation to a resolution of 1-km using cokriging with elevation as the covariate.

Analytical methods

Multicollinearity diagnosis between spatial covariates. To detect multicollinearity between all spatial covariates, we generated 1000 random points across the study area. To avoid spatial autocorrelation issues, the minimum distance between nearest points was constrained to be greater than 5 km. We then extracted the values of all spatial covariates into those 1000 points, and conducted a Pearson correlation analysis. The Pearson rank correlation matrix showed generally weak pairwise correlations between covariates ($r < 0.4$), except for FFMC and DMC ($r = 0.85$). Previous studies have shown that FFMC is a stronger predictor for the expected number of human-caused fires, whereas the DMC is a stronger predictor for the expected number of lightning-caused fires in boreal forest regions (Martell *et al*., 1989; Wotton *et al*., 2003). Therefore, we excluded DMC from analysis of human-caused fires and FFMC from analysis of lightning-caused fires. These 1000 random points was used for multicollinearity diagnosis only, and not used for subsequent analysis.

Exploratory analyses of the marginal effects of spatial covariates. For spatial categorical covariates (i.e. vegetation type, aspect, and landscape position), we graphically compared the observed fire frequencies (proportion of total number of fires that actually occurred for a variable class) and the expected fire frequencies (proportion of the study area in that variable class). Higher values than expected in a variable class identified that particular class to be more fire prone than others. We conducted a chi-square test of association for fire frequency among different classes.

For spatially continuous covariates, we used a lurking variable plot technique (Baddeley *et al*., 2005; Yang *et al*., 2007) to quantitate the effects of spatially continuous variables on fire occurrence pattern. This technique plots the cumulative Pearson residual of the complete spatial random (CSR) model against a continuous spatial covariate within a subregion to examine the systematic pattern of the covariate. The CSR model assumed the density of fire occurrence to be spatially stationary and thus did not account for any spatial covariate effects on fire occurrence pattern. Cumulative Pearson residual values should be approximately zero if the fitted null model explains almost all of the variation. If the cumulative Pearson residual value exceeds the two standard deviation error bounds line within a certain range of the variable, the analysis suggests there were more fires than the CSR model predicts in that particular variable range.

Quantitating the relationship between fire occurrence and spatial controls. To quantitate the relationship between fire occurrence and spatial controls, SPP analysis was performed using the R statistical package 'Spatstat' (Baddeley & Turner, 2005). A SPP is a data set $x = (x_1, \ldots, x_n)$ with n points observed in an observation window W. A spatial point process (e.g. Poisson, Cox, and Strauss process) is any stochastic mechanism that generates the SPP data x. The point process models fitted to the data are often formulated in terms of their Papangelou conditional density $\lambda(u; x)$, which may be loosely interpreted as the conditional probability of having an event at a point u ($u \in$W) given that the rest of the point process coincides with x (Baddeley & Turner, 2000). For the PPP, the conditional density function is the same as the density function $\lambda(u; x) = \lambda(u)$ because of the interactions among points was not considered in the PPP. In practice, the density function of PPP is often specified through a log-linear regression model as follows:

$$\lambda(u) = \exp(\theta_0 + \theta_1^* V_1 + \ldots + \theta_n^* V_n),$$

where $\lambda(u)$ is density at point u, which may be interpreted as the number of events that occurred per spatio-temporal unit. The $V_1 \ldots V_n$ are spatial covariates, and θ is the parameter vector (θ_0, θ_1, …, θ_n) to be estimated for the spatial covariates. The density $\lambda(u)$ will depend on θ to reflect 'spatial trend' (a change in density across the region of observation) or dependence on a covariate. The parameter vector θ was estimated via a maximum likelihood (Baddeley & Turner, 2000) implemented in the ppm() function of the 'Spatstat' package. For detailed description of the model fitting algorithm, refer to Appendix B.

In short, SPP analysis fits a spatial point process (e.g. PPP) that can generate the SPP data x, based on the effects of spatial covariates. Unlike conventional Poisson models in which the response variable is the number of events (e.g. fire counts) in each analysis areal unit, SPP analysis concerns with only the spatial information, and therefore can avoid the issues that are commonly related to the conventional Poisson modeling (e.g. zero inflation; R. Turner, pers. comm.).

To assess the relative importance of each spatial covariate, we constructed full inhomogeneous PPP models for human- and lightning-caused fires occurrence data with all spatial covariates (Table 1). For fire occurrence data, the SPP analysis only modeled the fire origin in the PPP, and did not consider the other properties (e.g. spread) of fires. We then compared the change in ΔAIC values caused by the removal of each individual covariate for human- and lightning-caused fires occurrence data. The change in AIC after removal of a single covariate gives an indication of the information lost due to its removal and can be used to measure the relative contribution of each covariate for human- and lightning-caused fires occurrence data, respectively.

Mapping the spatial distribution of current and future fire occurrence density. We used historical data to construct parsimonious models for predicting and mapping the distribution of human- and lightning-caused fires. Fire occurrence data were randomly divided into training data (80% of total fire occurrence data) and testing data (20% of total fire occurrence data). Training data were used to fit a parsimonious inhomogeneous PPP model and then map the spatial distribution of current fire occurrence density. Testing data were used to evaluate model performance. To capture the potentially nonlinear effects of spatial covariates on fire occurrence pattern, we considered second-order polynomial transformations of all spatial covariates and Cartesian coordinates (x,y) in the model selection procedure. Cartesian coordinates were included to account for spatial influences not represented in the set of measured covariates. We used AIC statistics (Burnham & Anderson, 2004) to select a parsimonious model where the model with the smallest AIC balances the best maximum likelihood fit to the data with a penalty term for increased model complexity (number of model parameters). The parsimonious model was selected by a backward-selection procedure. Parameters estimated from the final PPP model were used with covariates to predict and map the spatial distribution

Table 1 Spatial covariate datasets and sources

Variable	Abbreviation	Data source	Units
Biophysical factors			
Elevation	Elev	National Geomatics Center of China	Meter
Aspect	Asp	Derived from elevation	Class 1–3
Slope	Slope	Derived from elevation	Degree
Mean annual precipitation	Prep	China Meteorological Data Sharing Service system	mm
Mean annual temperature	Temp	China Meteorological Data Sharing Service system	°C
Vegetation type	Veg	Vegetation Map of The People's Republic of China (1 : 1 000 000)	Class 1–4
Topographic Position Index	TPI	Derived from elevation	Class 1–4
Fine fuel moisture content	FFMC*	Calculated based on algorithm described by Van Wagner (1987), daily meteorological data were downloaded from NCEP_Reanalysis data	Dimensionless (range: 0–101)
Duff moisture content	DMC†	The same as FFMC	Dimensionless (range: >0)
Lightning density	LightDen†	NASA Global Hydrology and Climate Centre Team	Flash rate per km^2 per year
Human factors			
Distance to nearest road	DisRd	National Geomatics Center of China	Meter
Distance to nearest settlement	DisSet	National Geomatics Center of China	Meter
Road density	RdDen	Derived from DisRd	km/km^2

*Variable was excluded from the lightning fire analysis.
†Variable was excluded from the human-caused fire analysis.

at 1-km resolution of fire occurrence density (number of fires to occur over a given spatio-temporal unit). The temporal extent of our PPP modeling is 45 years, matching the time period of our reported fire occurrences. Therefore, the estimated fire occurrence density was reported as number of fires per 1 km^2 per 45 years. For standardization, we multiplied our estimated fire occurrence density by 22.22 (1000/45) so that the reported unit became number of fires per 1000 km^2 per year.

We assessed the predictive performance of the most parsimonious model of human- and lightning-caused fires using the test data. We applied the validation method for resource selection functions (RSF) based on used vs. available sampling design proposed by Johnson *et al.* (2006). The validation method divided the predicted map into eight RSF bins and evaluated whether model predictions deviate from being proportional to the probability of use as required for an RSF. Linear regression and the chi-square test were applied to compare expected to observed probability of use. A model that was proportional to probability of use would have a slope of 1, an intercept of 0 and a high R^2 value with a nonsignificant chi-square goodness-of-fit value.

Parameters estimated from the most parsimonious model were also applied to future climate and fuel moisture contents to generate projections of the spatial distribution of fire occurrence density for the year 2100 under alternative GCM scenarios, whereas holding other variables constant. To highlight the climate change effects on fire occurrence density, the absolute difference in fire occurrence density between the two time periods was calculated as:

$$\Delta\lambda_{\text{change}} = \lambda_{\text{future}} - \lambda_{\text{current}},$$

where λ_{future} and λ_{current} represent fire occurrence density for 2100 and estimated for 1965–2009, respectively, and $\Delta\lambda_{\text{change}}$ represents fire occurrence density changes between current and alternative GCMs scenarios.

Finally, we summed fire occurrence density change for human- and lightning-caused fires on each cell. This led to a map of spatial distribution of overall fire occurrence density change, combined for both human- and lightning-caused fires. This map was used to evaluate the overall response of fire occurrence density to climate change.

Results

Spatial controls of human- and lightning-caused fire occurrence density

Spatial pattern of fire occurrences has been influenced by topographic variables and vegetation type, but not always in the same manner for human- and lightning-caused fires (Fig. 2). Aspect significantly affected human-caused fire occurrence density ($\chi^2 = 7.63$, df = 2, $P < 0.05$; Fig. 2a), but not lightning fire occurrence density ($\chi^2 = 4.41$, df = 2, $P = 0.11$; Fig. 2d). Observed human-caused fires occurred slightly more in xeric locations and less in mesic locations than expected given a null hypothesis of random occurrence (Fig. 2a). Vegetation type significantly affected both human-caused ($\chi^2 = 94.67$, df = 3, $P < 0.0001$; Fig. 2b) and lightning fire occurrence density ($\chi^2 = 17.43$, df = 3, $P < 0.0001$; Fig. 2e). Vegetation type showed contrasting effects on human- vs. lightning-caused fires. For example, expected human-caused fires were significantly higher in broadleaf forests and meadows, and lower than expected in coniferous and mixed forests (Fig. 2b). On the contrary, expected lightning fires were significantly higher in coniferous forests, and lower than expected in meadows (Fig. 2e). Landscape position also significantly affected both human-caused ($\chi^2 = 8.34$, df = 3, $P < 0.05$; Fig. 2c), and lightning fire occurrence density ($\chi^2 = 11.01$, df = 3, $P < 0.05$; Fig. 2f). Observed human-caused fires were less frequent on ridge tops than expected (Fig. 2c). Conversely, observed lightning fires were more frequent on ridge tops than expected (Fig. 2f).

Lurking variable techniques revealed that cumulative Pearson residuals are significant (i.e. larger than the 2σ limit) when distance to the nearest road is less than 10 km, distance to the nearest settlement is less than 20 km, elevation is between 500 and 800 m, and slope is less than 4° for human-caused fires (Fig. 3a–d). This suggests that there are more human-caused fires occurring at locations that fall within these bounds than the null model predicts. Although these four covariates influence lightning fire patterns, their effects on fire occurrence pattern do not reach to significant level (i.e. within the 2σ limit; Fig. 3e–f).

The delta AIC method showed that the relative importance of covariates for human- vs. lightning-caused fire occurrence pattern was quite different (Appendix A3). For human-caused fires, variables indicating human accessibility (distance to the nearest road and settlement, and road density) exerted the greatest influence, followed by fine fuel moisture contents and vegetation type, and then climate and biophysical factors. For lightning fires, duff moisture contents and vegetation type exerted the greatest influence, followed by slope, temperature, and lightning density, and then variables indicating human accessibility (distance to the nearest road and settlement, and road density).

Spatial distribution of current fire occurrence density

The estimated current human-caused fire occurrence density (λ_{CHF}) ranged between 0.0144 and 0.55 fires per 1000 km^2 per year, with a median value of 0.168 fires per 1000 km^2 per year. The spatial distribution of λ_{CHF} was highly heterogeneous across the landscape due to the effects of human accessibility. High λ_{CHF} areas were distributed mainly along the road networks, suggesting

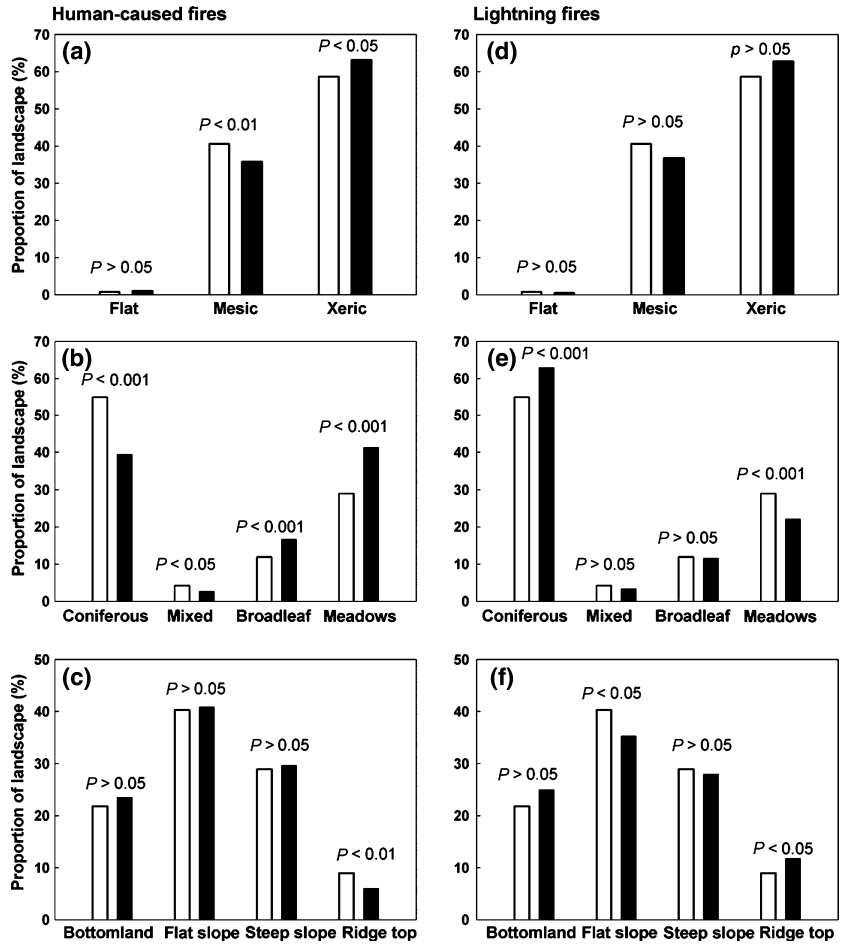

Fig. 2 Proportion of observed frequency (solid bars) and available areas (expected fire occurrence, open bars) for human-caused fire occurrence: (a) aspect, (b) vegetation type, and (c) topographic position, and lightning fire occurrence: (d) aspect, (e) vegetation type, and (f) topographic position. *P*-value was reported from chi-square test to examine differences in fire frequency among the different categories.

strong effects of human activity on the distribution of fire occurrence (Fig. 4a). The estimated current lightning fire occurrence density (λ_{CLF}) ranged between 0.00375 and 0.28 fires per 1000 km^2 per year, with a median value of 0.160 fires per 1000 km^2 per year. The spatial distribution of λ_{CLF} was quite different from that of λ_{CHF} (Fig. 4b). We examined the correlation between λ_{CLF} with spatial covariates, and found a strongest correlation between λ_{CLF} and elevation. Visual examination also revealed that the spatial pattern of λ_{CLF} was similar to spatial variation of elevation across the study area (Appendix A4; Fig. 4b).

We used test data to validate our predictive maps for λ_{CHF} and λ_{CLF}. For human-caused fire, the regression model suggested that the fitted PPP model was reasonable, with a slope (1.12) close to 1, and an intercept (−0.015) close to 0, and with $R^2 = 0.95$. The chi-square goodness-of-fit test resulted in a nonsignificant difference between observed and expected probability of use ($\chi^2 = 2.55$, df = 7, $P = 0.923$). For lightning fire, the regression model suggested that the fitted PPP model was also reasonable, with a slope (1.18) close to 1, and an intercept (−0.023) close to 0, and with $R^2 = 0.71$. The chi-square goodness-of-fit test resulted in a nonsignificant difference between observed and expected probability of use ($\chi^2 = 4.78$, df = 7, $P = 0.71$). This suggests that the fitted PPP model effectively quantifies the underlying causal relationships influencing the human- and lightning-caused fire patterns.

We combined the map of λ_{CHF} and λ_{CLF} to show the spatial distribution of overall fire occurrence density (λ_{COF}). The estimated λ_{COF} ranged between 0.011 and 0.82 fires per 1000 km^2 per year, with a median value of 0.36 fires per 1000 km^2 per year. Because most fires were caused by anthropogenic factors, spatial distribution of λ_{COF} was also highly related to human accessibility. High λ_{COF} areas were distributed mainly along the road networks (Fig. 4c).

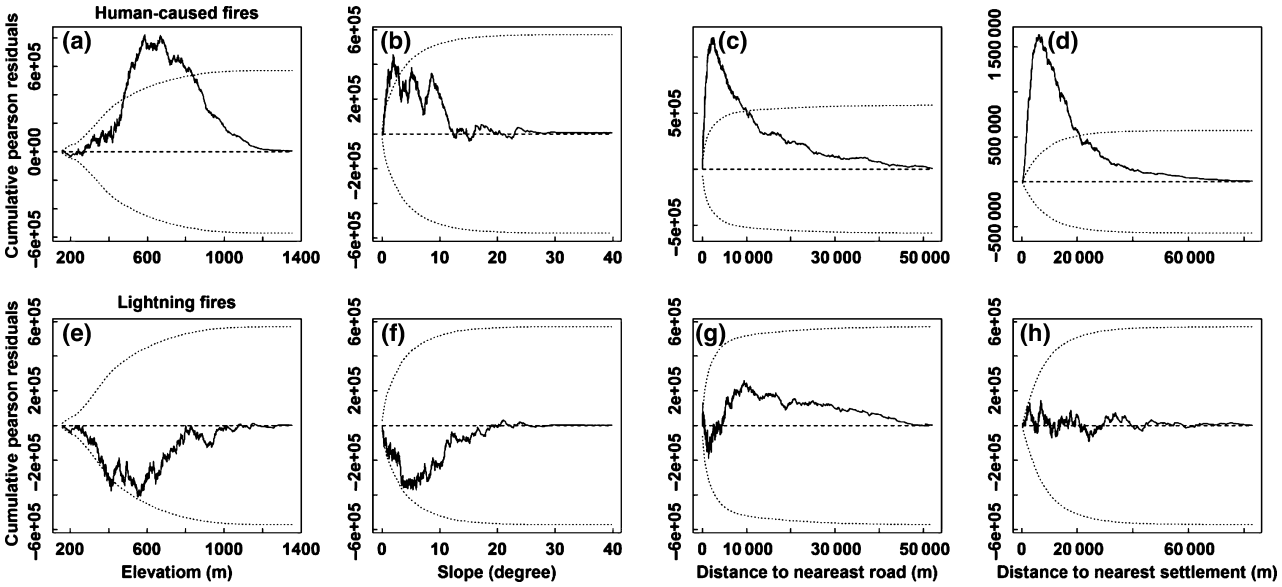

Fig. 3 Lurking variable plots against (a) elevation, (b) slope, (c) distance to the nearest road, and (d) distance to the nearest settlement for the null model of human-caused fire data, and (e) elevation, (f) slope, (g) distance to the nearest road, and (h) distance to the nearest settlement for the null model of lightning fire data. The solid lines are empirical curves of cumulative Pearson residuals. The dotted lines denote two-standard-deviation error bounds. The dashed lines indicate the zero intercept.

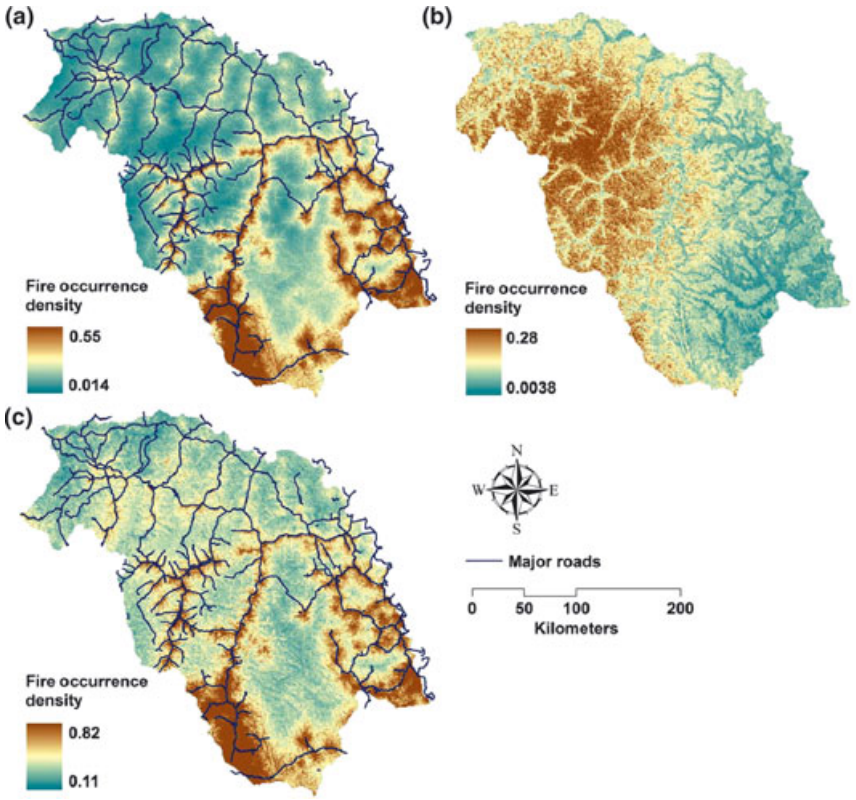

Fig. 4 Map of estimated current occurrence density for (a) human-caused fires, (b) lightning fires, and (c) all fires, overlaid with major roadway coverage. Fire occurrence density was defined as the number of fires per 1000 km^2 per year. Note the scale changes in symbology bar.

Effects of climate change on the spatial distribution of fire occurrence density

Annual temperature and precipitation were predicted to increase under all GCM scenarios in our study area (Appendix A5). Under both GCMs, the magnitude of annual temperature and precipitation change was smaller under the B1 emission scenario than the A2 scenario. Both increased temperature and precipitation exhibited a latitudinal gradient, with the greatest increase occurring in the northern area of the Great Xing'an Mountains, which is consistent with both weather station data and model prediction results (Qin *et al*., 2005; Wang *et al*., 2006).

The final PPP model indicated that annual temperature and fuel moisture contents had positive linear effects on both human- and lightning-caused fire occurrence (Table 2). Precipitation had positive linear effects on human-caused fire, but exerted reverse hyperbolic effects on lightning fire. Increased precipitation would initially increase, but then gradually decrease the spatial probability of lightning fire occurrence (Table 2). In general, both spatial distribution of future human-caused fire occurrence density (λ_{FHF}) and lightning fire occurrence density (λ_{FLF}) under all GCM scenarios displayed a pattern similar to that of the current distribution, but with greater occurrence density (Fig. 4; Appendix A6 and A7). Fire occurrence density for both categories was predicted to increase for each cell on the landscape, but the overall increase had a very heterogeneous distribution (Figs 5 and 6). Response of fire occurrence density for both categories was positively related to degree of climate change (Figs 5 and 6; Appendix A5). For example, both the greatest increase in fire occurrence density and annual temperature and precipitation were predicted under the HadCM3 A2 scenario. Conversely, the smallest increases in fire occurrence density, annual temperature, and precipitation were predicted under the CGCM3 B1 scenario.

Both $\Delta\lambda_{HF}$ and $\Delta\lambda_{LF}$ showed a heterogeneous distribution across the landscape, but their spatial pattern were highly inconsistent. For human-caused fires, the areas with the greatest occurrence density change were distributed along the current road networks, which coincided with the area most accessible to humans (Fig. 5). However, the percentage change of spatial distribution of $\Delta\lambda_{HF}$ showed a latitudinal gradient, consistent with climate change influences (Appendix A5 and 8). For lightning fires, the areas with the greatest occurrence density change were distributed in the northern part of the study area, which coincided with the greatest predicted increases of annual temperature and precipitation.

For overall (human- + lightning-caused) fires, the areas with the greatest overall fire occurrence density change were distributed in the northern part of the study area, which is contributed by increased lightning fires; and along the current road networks, which is contributed by increased human-caused fires (Fig. 7; Appendix A5).

Table 2 Coefficients of the selected predictor variables and their transformation for the selected most parsimonious model of human- and lightning-caused fires

Human-caused fires Parameter (function)	Coefficient	Lightning fires Parameter (function)	Coefficient
Intercept	−37.84	Intercept	51.05
X	-1.258×10^{-5}	X	-3.598×10^{-6}
Y	1.606×10^{-6}	Y	-1.351×10^{-5}
Elev	-5.194×10^{-3}	Elev	0.004
factor(TPI)-flat slope	−0.0196	factor(TPI)-flat slope	−0.240
factor(TPI)-steep slope	0.315	factor(TPI)-steep slope	−3.087
factor(TPI)-ridge top	0.470	factor(TPI)-ridge top	−0.192
factor(Asp)-mesic	−0.340	factor(Asp)-mesic	0.677
factor(Asp)-xeric	−0.234	factor(Asp)-xeric	0.846
factor(Veg)-mixed forest	−0.318	factor(Veg)-mixed forest	−0.222
factor(Veg)-broadleaf forest	−0.0801	factor(Veg)-broadleaf forest	−0.077
factor(Veg)-meadows	−0.0124	factor(Veg)-meadows	−0.333
Prep	0.0310	Prep	0.0177
Temp	0.115	Prep^2	-7.406×10^{-6}
FFMC	0.118	Temp	0.117
DisSet	-8.183×10^{-5}	DMC	0.133
DisSet^2	1.138×10^{-9}	LightDen	0.425
DisRd^2	-3.927×10^{-10}		
RdDen	0.101		

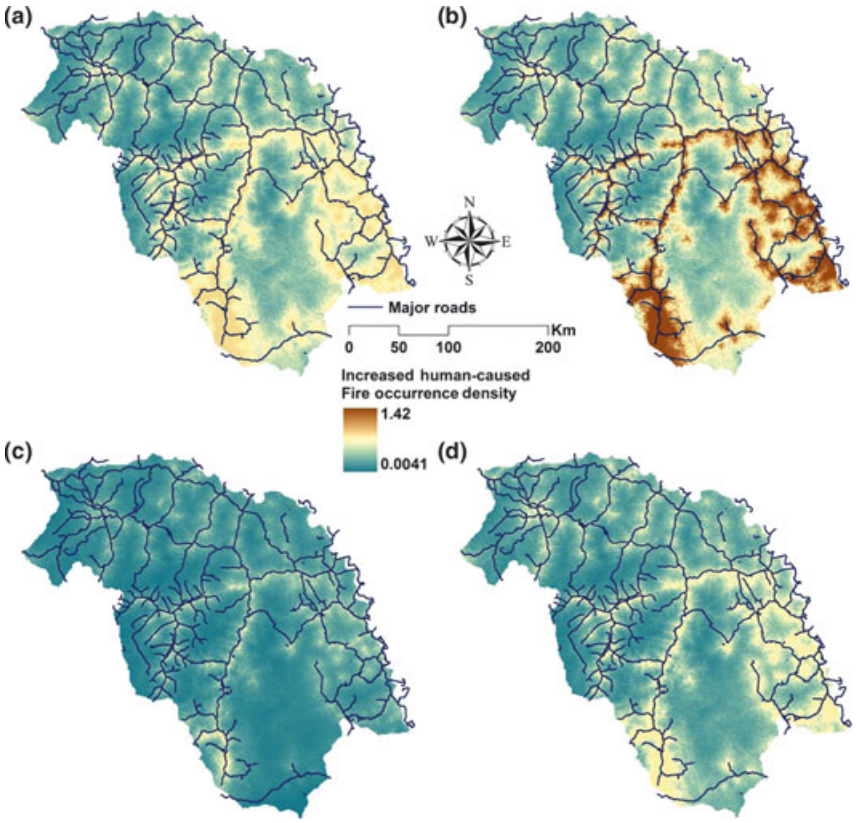

Fig. 5 Spatial distributions of differences in human-caused fire occurrence density ($\Delta\lambda_{HF}$) between current climate and alternative future climate scenarios of (a) CGCM A2, (b) HadCM A2, (c) CGCM B1, and (d) HadCM B1. Current major roadway coverage is overlaid. Fire occurrence density is defined as the number of fire occurrences per 1000 km^2 per year.

Discussion

Climate change vs. anthropogenic effects on spatial distribution of fire occurrence density

Our analysis found that climate change is likely to significantly increase the occurrence density of both human- and lightning-caused fires. The magnitude of increase is expected to vary spatially across the landscape (Figs 5–7). The spatial patterns of the increase are consistent with the spatial patterns of climate change for the lightning-caused fires (Fig. 6 vs. Appendix A5), but inconsistent for the human-caused fires (Fig. 5 vs. Appendix A5). In comparison, spatial patterns of relative increase in fire occurrence density are consistent with climate change patterns for both human- and lightning-caused fire (Appendix A8 and 9). This suggests that climate change is the main driver of the change of fire occurrence density in our analysis. However, because a small relative change in the hotspots can lead to a large absolute change due to very large fire occurrence densities in those hotspots, the spatial distribution of changed and future hotspots of human-caused fire occurrence density will likely remain distributed similarly as currently, and will remain concentrated along the clustered and linear components of human infrastructure (Figs 4a and 5; Appendix A6). The fact the climate change was not predicted to result in a major shift in fire occurrence hotspots patterns suggested that climate change effects on the spatial distribution of fire occurrence density may never outweigh that resulting from anthropogenic factors for the next 100 years. Thus, the legacy effects exerted by human infrastructure on fire occurrence density may last throughout the 21th century. Our results suggest that the response of fire to climate is strongly constrained by patterns of human activity in this human-dominated forest landscape. In this light, accurate projection of fire response to climate change in areas of substantial human influence should incorporate historical, current, and if possible, future patterns of human activity.

Our analysis found that temperature and fuel moisture had positive effects on both human- and lightning-caused fire occurrence. Increased temperatures had a positive effect on fire occurrence, likely because higher temperatures will result in drier fuels, longer fire

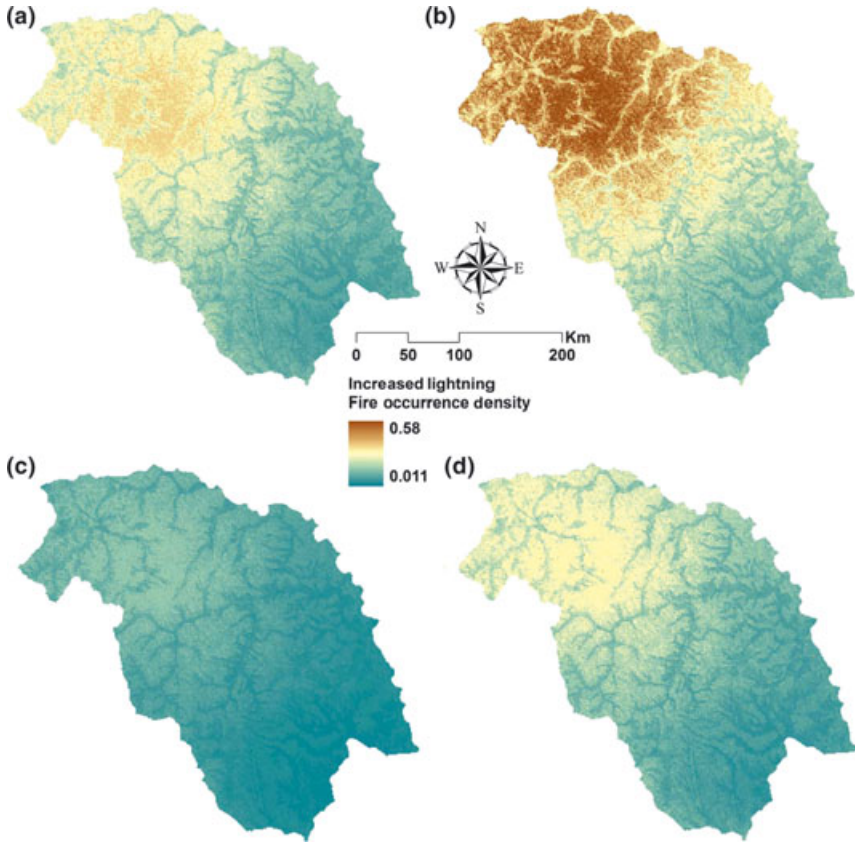

Fig. 6 Spatial distributions of differences in lightning-caused fire occurrence density ($\Delta\lambda_{LF}$) between current climate and alternative future climate scenarios of (a) CGCM A2, (b) HadCM A2, (c) CGCM B1, and (d) HadCM B1. Fire occurrence density is defined as the number of fire occurrences per 1000 km^2 per year.

seasons, and more intense fire weather conditions (Meehl & Tebaldi, 2004; Arienti *et al.*, 2006). Fuel availability may also increase because of increased photosynthesis resulting from the effects of elevated temperature and CO_2 concentrations on the rates of plant growth and water use efficiency in boreal forests (Chapin *et al.*, 2002; Luo *et al.*, 2006). Fuel moisture code may increase, leading to increased ignition probability, because the increased temperature may enhance evapotranspiration not compensated for by increasing precipitation in the boreal forest (Meehl & Tebaldi, 2004). Overall, these combined effects may lead to more continuous and drier fuels and increased fire risk overall. Climate change (and even fire itself) may also change the species composition of the forests and thus further alter fire regimes in ways that are hard to predict. Furthermore, the predicted increase of precipitation occurs mostly in autumn and winter (IPCC, 2007), beyond the main fire season for our study region (Tian *et al.*, 2011). For example, from 1965–2009 only 15.3% of fires in the Great Xing'an Mountains occurred in autumn and winter. Although precipitation had a lagged effect on fuel moisture, such effect only lasted for a short periods of time because current fuel moisture was influenced by preceding day's climate conditions. Therefore, projected increases in precipitation may contribute little to increased fuel moisture in the fire season. Our statistical analysis also revealed that precipitation has a nonlinear effect on lightning fire occurrence. Increased precipitation will initially exert a positive effect on fire occurrence, possibly due to increased lightning density (Tapia *et al.*, 1998). Nonetheless, an excessive increase in precipitation may reduce lightning fire occurrence, possibly due to higher fuel moisture content (Van Wagner, 1987). On an overall basis, determining the balance of forces for increasing or decreasing lightning fire occurrence resulting from increased lightning density or fuel moisture content remains elusive and requires further investigation.

Human-caused fire constituted the majority of fire in the study area, which is more heavily populated than most boreal forests of the world. Understanding the influence of human activities on the distribution of fire occurrence is therefore central to mitigate fire risk in

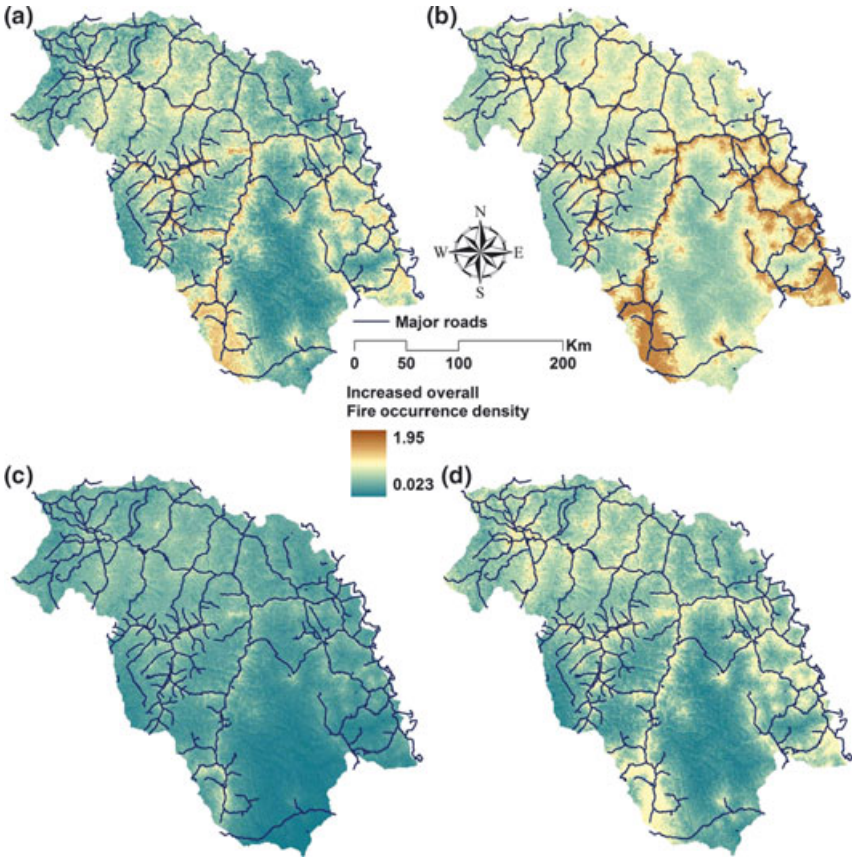

Fig. 7 Spatial distributions of differences in overall (human- + lightning-caused) fire occurrence density ($\Delta\lambda_{OF}$) between current climate and alternative future climate scenarios of (a) CGCM A2, (b) HadCM A2, (c) CGCM B1, and (d) HadCM B1. Current major roadway coverage is overlaid. Fire occurrence density is defined as the number of fire occurrences per 1000 km^2 per year.

the presence of rapid changes in land use and climate. Our results demonstrated that spatial patterns of all fire occurrence density was strongly associated with human accessibility to natural landscapes, with road density and proximity to settlements and roads found to be the most important factors. This suggests that human development and activity patterns are beginning to override the biophysical factors that historically have controlled fire regimes in the Great Xing'an Mountains.

Effects of biophysical factors on fire occurrence density

Vegetation type varied in its relative importance and effect on human- vs. lightning-caused fires in our study area. Generally, vegetation type had a small importance in explaining spatial pattern of human- and lightning-caused fire occurrence density, as indicated by relatively small delta AIC value. This may be because that fuel is generally not considered a limiting factor in boreal forest (Johnson & Larsen, 1991). Our field investigations have also shown that fine fuel loadings on the forest floor may not differ significantly among the various vegetation types (Chen *et al*., 2008; Liu *et al*., 2008). Furthermore, the Black Dragon Fires, which burned almost one eighth of the total study area, may contribute to the homogeneity of surface fuels. However, the relative importance of vegetation type is much smaller for human-caused fires, due to the overwhelming effects of anthropogenic effects, than that for lightning fires.

Our results revealed contrasting effects of vegetation type on lightning- vs. human-caused fires. Lightning fires were significantly higher in coniferous forests (Fig. 2e). Many studies have demonstrated that forest type significantly affected fire occurrence (Bergeron *et al*., 2004), and conifer-dominated stands, due to higher flammability of surface fuels, general exhibited higher fire frequency than broadleaf forests (Hély *et al*., 2000; Krawchuk *et al*., 2006). However, for human-caused fire, broadleaf forests and meadows displayed a higher mean occurrence density, of 0.302 fires per 1000 km^2 per year in broadleaf forest and meadows vs. 0.153 fires per 1000 km^2 per year in coniferous forests (Fig. 2b). This may be due to the following two reasons.

First, as our results have shown, human-caused fires will most likely occur near cultural features. For example, the areas within a distance of 2000 m from roads accounted for 38.6% of human-caused fires, but only accounted for 24.4% in area. These areas are the most disturbed forested areas, which have a much higher proportion of broadleaf tree species or meadows (50.5%), compared with areas at a distance greater than 2000 m from roads (37.7%). Second, our vegetation map was produced in 1982. Fire-disturbed areas before 1982 may have regenerated as early successional broadleaf tree species or as meadow vegetation, which is recorded by VMPRC. However, these areas may have been dominated by other vegetation types when fire actually occurred. Our analysis indicated that fire occurrence was not significantly different among different forest types before and after 1983 ($\chi^2 = 5.39$, df = 3, $P = 0.15$; Appendix A10). This suggests that high human-caused fire occurrence density in broadleaf forests and meadows has resulted primarily from anthropogenic forest type conversions, such as increased grass cover near roads leading to increased availability of flammable fine fuels (Arienti *et al.*, 2009).

Caveats

There are two main limitations regarding the use of fire atlases to extrapolate long-term patterns of fire occurrence using empirical models. The first concerns the quality of fire database. Long-term fire databases may be subject to bias because of changes in fire management policy, different recorders, and the legacy of past management practices. The other limitation involves the selection of spatial covariates appropriate for such a long study period. Ideally, we should examine the relationship among fire and spatial covariates at the time of fire occurrences. However, spatial covariates are complex and change frequently during the time span encompassed by a fire database. For example, the Black Dragon Fire has drastically changed the vegetation type and forest management policy in this region. However, the scarcity of data in our study area limited our selection of spatial covariates such as vegetation type and human factors to only one time period. Despite these limitations, fire databases still represent a useful source of historical information that enabled the spatial analysis of fire and its controlling factors in our research area, given the lack of data from fire-scarred trees in this region. Empirical analyses of relationships among fire and various spatial controls provided insights on fire management and the potential response of fire to changing climate.

When considering the future spatial distribution of human-caused fire occurrence density, it is important to identify the covariates that are likely to change overtime. Anthropogenic drivers are likely to be modified in the future through increased settlement, road network expansion, and other development processes. Human factors may exert an even stronger influence on spatial patterns of wildfire ignition in the future, due to predicted increasing trends in China's human population (National Bureau of Statistics of China, 2010). Our projection of future lightning fire occurrence density did not explicitly account for change in lightning activity, which is closely related to climate (Tapia *et al.*, 1998; Reeve & Toumi, 1999). Moreover, we used a single best model, rather than ensemble forecasting of multiple models (Araújo & New, 2007), to project future occurrence density. All these factors will introduce uncertainties in the results. Thus, our projection of future fire occurrence should not be regarded in the sense of an accurate prediction, but rather as a representation of the response of future fire occurrence caused by climate change. Although failure to incorporate future changes in human development processes and lightning activity may hinder our interpretation of predictions, our results strongly suggest that the response of fire occurrence in Chinese boreal forests to future climate will be more constrained by anthropogenic factors than by climate change.

Acknowledgements

This research was funded by National Natural Science Foundation of China (41071121 & 31100345) and the Hundred Talent Program of Chinese Academy of Sciences. YC also acknowledges the support from the NSFC grant 31070422. We thank Mr. Tom Dilts for providing valuable comments on earlier drafts, Dr. Rolf Turner for helpful discussion about the spatial point pattern analysis, Dr. Bernald Lewis for editing our manuscript, and Dr. Inmaculada Aguado for providing the MFDIP program, which made the calculation of fuel moisture code possible. The constructive comments of five anonymous referees greatly improved the manuscript.

Author contributions: Z. L. led the analysis of the fire ignition data and the writing of the manuscript. J. Y. designed the project, oversaw the analysis, and contributed to the R coding and the writing of the manuscript. Y. C. led the acquisition of the fire ignition data. P. J. W. and H. S. H. contributed to the writing of the manuscript.

References

Araújo MB, New M (2007) Ensemble forecasting of species distributions. *Trends in Ecology and Evolution*, **22**, 42–47.

Arienti MC, Cumming SG, Boutin S (2006) Empirical models of forest fire initial attack success probabilities: the effects of fuels, anthropogenic linear features, fire weather, and management. *Canadian Journal of Forest Research*, **36**, 3155–3166.

Arienti MC, Cumming SG, Krawchuk MA, Boutin S (2009) Road network density correlated with increased lightning fire incidence in the Canadian western boreal forest. *International Journal of Wildland Fire*, **18**, 970–982.

Baddeley A, Turner R (2000) Practical maximum pseudolikelihood for spatial point patterns. *Australian and New Zealand Journal of Statistics*, **42**, 283–322.

Baddeley A, Turner R (2005) Spatstat: an R package for analyzing spatial point patterns. *Journal of Statistical Software*, **12**, 1–42.

Baddeley A, Turner R, Moller J, Hazelton M (2005) Residual analysis for spatial point processes. *Journal of the Royal Statistical Society Series B-Statistical Methodology*, **67**, 617–651.

Bergeron Y, Gauthier S, Flannigan M, Kafka V (2004) Fire regimes at the transition between mixedwood and coniferous boreal forest in northwestern Quebec. *Ecology*, **85**, 1916–1932.

Bessie W, Johnson E (1995) The relative importance of fuels and weather on fire behavior in subalpine forests. *Ecology*, **76**, 747–762.

Bond-Lamberty B, Peckham S, Ahl D, Gower S (2007) Fire as the dominant driver of central Canadian boreal forest carbon balance. *Nature*, **450**, 89–92.

Bu RC, He HS, Hu YM, Chang Y, Larsen DR (2008) Using the LANDIS model to evaluate forest harvesting and planting strategies under possible warming climates in Northeastern China. *Forest Ecology and Management*, **254**, 407–419.

Burnham KP, Anderson DR (2004) Multimodel inference: understanding AIC and BIC in Model Selection. *Sociological Methods and Research*, **33**, 261–304.

Cary GJ, Keane RE, Gardner RH *et al*. (2006) Comparison of the sensitivity of landscape-fire-succession models to variation in terrain, fuel pattern, climate and weather. *Landscape Ecology*, **21**, 121–137.

Chang Y, He HS, Bishop I, Hu YM, Bu RC, Xu CG, Li XZ (2007) Long-term forest landscape responses to fire exclusion in the Great Xing'an Mountains, China. *International Journal of Wildland Fire*, **16**, 34–44.

Chapin FS, Matson PA, Mooney HA (2002) *Principles of Terrestrial Ecosystem Ecology*. Springer Verlag, New York, NY, USA.

Chen H, Chang Y, Hu Y M *et al*. (2008) Load of forest surface dead fuel in Huzhong area of Daxing'anling Mountains and relevant affecting factors. *Chinese Journal of Ecology*, **27**, 50–55.

Christian HJ, Blakeslee RJ, Boccippio DJ *et al*. (2003) Global frequency and distribution of lightning as observed from space by the Optical Transient Detector. *Journal of Geophysical Research*, **108**, 4005, doi: 10.1029/2002JD002347

Daniau AL, Harrison SP, Bartlein PJ (2010) Fire regimes during the Last Glacial. *Quaternary Science Reviews*, **29**, 2918–2930.

Dissing D, Verbyla DL (2003) Spatial patterns of lightning strikes in interior Alaska and their relations to elevation and vegetation. *Canadian Journal of Forest Research*, **33**, 770–782.

Editorial Committee of Vegetation Map of China (2007) *Vegetation Map of China and Its Geographic Pattern-Illustration of Vegetation Map of the People's Republic of China (1 : 1 000 000)*. Geology Press House, Beijing (in Chinese).

Falk DA, Heyerdahl EK, Brown PM *et al*. (2011) Multi-scale controls of historical forest-fire regimes: new insights from fire-scar networks. *Frontiers in Ecology and the Environment*, **9**, 446–454.

Fang J, Chen A, Peng C, Zhao S, Ci L (2001) Changes in forest biomass carbon storage in China between 1949 and 1998. *Science*, **292**, 2320–2322.

Fauria M, Johnson E (2006) Large-scale climatic patterns control large lightning fire occurrence in Canada and Alaska forest regions. *Journal of Geophysical Research*, **111**, G04008, doi: 10.1029/2006JG000181

Flannigan MD, Wotton M (2001) Climate, weather, and area burned. In: *Forest Fires: Behavior and Ecological Effects* (eds Johnson ED, Miyanishi K), pp. 351–377. Academic Press, San Diego, CA.

Flannigan MD, Stocks B, Turetsky M, Wotton M (2009a) Impacts of climate change on fire activity and fire management in the circumboreal forest. *Global Change Biology*, **15**, 549–560.

Flannigan MD, Krawchuk MA, De Groot WJ, Wotton BM, Gowman LM (2009b) Implications of changing climate for global wildland fire. *International Journal of Wildland Fire*, **18**, 483–507.

Girardin MP, Mudelsee M (2008) Past and future changes in Canadian boreal wildfire activity. *Ecological Applications*, **18**, 391–406.

Hély C, Bergeron Y, Flannigan M (2000) Effects of stand composition on fire hazard in mixed-wood Canadian boreal forest. *Journal of Vegetation Science*, **11**, 813–824.

Hou X, Sun S, Zhang J, He M, Wang Y, Kong D, Wang S (1982) *Vegetation Map of the People's Republic of China*. China Cartography, Beijing (in Chinese).

IPCC (2007) Climate change 2007: synthesis report. In: *Contribution of Working Groups I II and III to the Fourth Assessment Report of the Intergovernmental Panel on Climate Change*. Intergovernmental Panel on Climate Change, Geneva, Switzerland.

Jenness J (2005) *Topographic Position Index (tpi_jen. avx) Extension for ArcView 3. x*. Jenness Enterprises, Flagstaff, AZ, USA, pp. 1–42.

Johnson EA, Larsen C (1991) Climatically induced change in fire frequency in the southern Canadian Rockies. *Ecology*, **72**, 194–201.

Johnson C, Nielsen S, Merrill E, Mcdonald T, Boyce M (2006) Resource selection functions based on use-availability data: theoretical motivation and evaluation methods. *The Journal of Wildlife Management*, **70**, 347–357.

Johnstone J, Hollingsworth T, Chapin F III, Mack M (2010) Changes in fire regime break the legacy lock on successional trajectories in Alaskan boreal forest. *Global Change Biology*, **16**, 1281–1295.

Krawchuk M, Cumming S, Flannigan M, Wein R (2006) Biotic and abiotic regulation of lightning fire initiation in the mixedwood boreal forest. *Ecology*, **87**, 458–468.

Krawchuk MA, Cumming SG, Flannigan MD (2009a) Predicted changes in fire weather suggest increases in lightning fire initiation and future area burned in the mixedwood boreal forest. *Climatic Change*, **92**, 83–97.

Krawchuk MA, Moritz MA, Parisien MA, Van Dorn J, Hayhoe K (2009b) Global pyrogeography: the current and future distribution of wildfire. *PLoS ONE*, **4**, e5102.

Lafon CW, Grissino-Mayer HD (2007) Spatial patterns of fire occurrence in the central Appalachian mountains and implications for wildland fire management. *Physical Geography*, **28**, 1–20.

Li Y, Hu Y, Chang Y, Xu C, Li X, Bu R, He HS (2006) Forest landscape change and driving forces in Huzhong Forest Bureau of Daxing'anling in China. *Acta Ecologica Sinica*, **26**, 3347–3357.

Liu Z, Chang Y, Chen H, Zhou R, Jing G, Zhang H, Zhang C (2008) Spatial pattern of land surface dead combustible fuel load in Huzhong forest area in Great Xing'an Mountains. *Chinese Journal of Applied Ecology*, **19**, 487–493.

Liu H, Bu R, Liu J, Leng W, Hu Y, Yang L (2011) Predicting the wetland distributions under climate warming in the Great Xing'an Mountains, Northeastern China. *Ecological Research*, **26**, 605–613.

Luo Y, Hui D, Zhang D (2006) Elevated CO_2 stimulates net accumulations of carbon and nitrogen in land ecosystems: a meta-analysis. *Ecology*, **87**, 53–63.

Marlon J, Bartlein P, Carcaillet C *et al*. (2008) Climate and human influences on global biomass burning over the past two millennia. *Nature Geoscience*, **1**, 697–702.

Martell DL, Bevilacqua E, Stocks BJ (1989) Modelling seasonal variation in daily people-caused forest fire occurrence. *Canadian Journal of Forest Research*, **19**, 1555–1563.

Meehl GA, Tebaldi C (2004) More intense, more frequent, and longer lasting heat waves in the 21st century. *Science*, **305**, 994–997.

Mitchener L, Parker A (2005) Climate, lightning, and wildfire in the national forests of the southeastern United States: 1989–1998. *Physical Geography*, **26**, 147–162.

Nakicenovic N, Alcamo J, Davis G (2000) *Special Report on Emissions Scenarios: A Special Report of Working Group III of the Intergovernmental Panel on Climate Change*. Cambridge University Press, New York, NY.

National Bureau of Statistics of China (2010) *China Statistical Yearbook 2010*. China Statistics Press, Beijing.

Nemani RR, Keeling CD, Hashimoto H *et al*. (2003) Climate-driven increases in global terrestrial net primary production from 1982 to 1999. *Science*, **300**, 1560–1563.

Parisien M-A, Moritz MA (2009) Environmental controls on the distribution of wildfire at multiple spatial scales. *Ecological Monographs*, **79**, 127–154.

Pechony O, Shindell D (2010) Driving forces of global wildfires over the past millennium and the forthcoming century. *Proceedings of the National Academy of Sciences of the United States of America*, **107**, 19167–19170.

Qin D, Ding Y, Su JL *et al*. (2005) Assessment of climate and environment changes in China (I): climate and environment changes in China and their projection. *Advances in Climate Change*, **1**, 4–9.

Reeve N, Toumi R (1999) Lightning activity as an indicator of climate change. *Quarterly Journal of the Royal Meteorological Society*, **125**, 893–903.

Rollins MG, Morgan P, Swetnam T (2002) Landscape-scale controls over 20(th) century fire occurrence in two large Rocky Mountain (USA) wilderness areas. *Landscape Ecology*, **17**, 539–557.

Scholze M, Knorr W, Arnell NW, Prentice IC (2006) A climate-change risk analysis for world ecosystems. *Proceedings of the National Academy of Sciences of the United States of America*, **103**, 13116–13120.

Syphard AD, Radeloff VC, Keeley JE, Hawbaker TJ, Clayton MK, Stewart SI, Hammer RB (2007) Human influence on california fire regimes. *Ecological Applications*, **17**, 1388–1402.

Tapia A, Smith JA, Dixon M (1998) Estimation of convective rainfall from lightning observations. *Journal of Applied Meteorology*, **37**, 1497–1509.

Tian X, McRae DJ, Jin J, Shu L, Zhao F, Wang M (2011) Wildfires and the Canadian Forest Fire Weather Index system for the Daxing'anling region of China. *International Journal of Wildland Fire*, **20**, 963–973.

Van Wagner C (1987) *Development and Structure of the Canadian Forest Fire Weather Index System*. Forestry technical report FTR-35, Canadian Forestry Service, Petawawa National Forestry Institute, Chalk River, Ontario, 36 pp.

Wang Y, Cao M, Tao B, Li K (2006) The characteristics of spatio-temporal patterns in precipitation in China under the background of global climate change. *Geographic Research*, **25**, 1031–1040.

Westerling A, Hidalgo H, Cayan D, Swetnam T (2006) Warming and earlier spring increase western US forest wildfire activity. *Science*, **313**, 940–943.

Williams ER (2005) Lightning and climate: a review. *Atmospheric Research*, **76**, 272–287.

Wotton BM, Martell DL, Logan KA (2003) Climate change and people-caused forest fire occurrence in Ontario. *Climatic Change*, **60**, 275–295.

Wotton BM, Nock CA, Flannigan MD (2010) Forest fire occurrence and climate change in Canada. *International Journal of Wildland Fire*, **19**, 253–271.

Xu HC (1998) *Forest in Great Xing' An Mountains of China*. Science Press, Beijing.

Xu CH, Li ZD, Qiu Y (1997) Fire disturbance history in virgin forest in northern region of Daxing'anling mountains. *Acta Ecologica Sinica*, **17**, 3–9.

Yang J, He HS, Shifley SR, Gustafson EJ (2007) Spatial patterns of modern period human-caused fire occurrence in the Missouri Ozark Highlands. *Forest Science*, **53**, 1–15.

Yang J, He HS, Shifley SR (2008) Spatial controls of occurrence and spread of wildfires in the missouri ozark highlands. *Ecological Applications*, **18**, 1212–1225.

Zhao M, Running SW (2010) Drought-induced reduction in global terrestrial net primary production from 2000 through 2009. *Science*, **329**, 940–943.

Zhou YL (1991) *Vegetation in Great Xing' An Mountains of China*. Science Press, Beijing.

Zhou D (2007) *Potential Responses of Major Species and Forest Types to Climate Change in Small Xing'an Mountains*. Unpublished Ph.D Dissertation, Institute of Applied Ecology, Chinese Academy of Sciences, Shenyang, China, 169 pp.

Supporting Information

Additional Supporting Information may be found in the online version of this article:

Appendix A1. The annual temporal variation of fire counts and burned area for lightning- and human-caused fires.
Appendix A2. Examinations of whether there is a significant difference between projected historical' (CGCM3-20C3M) and recorded climate from 1965 to 2000.
Appendix A3. Change in AICc (ΔAICc) resulting from removal of individual covariates from the full PPP model of human- and lightning-caused fires (ΔAICc in descending order).
Appendix A4. Digital elevation model for the study area.
Appendix A5. Spatial distribution of difference in annual temperature and precipitation between projected historical' (the 20C3M scenario from 1960 to 2000) and future (2081–2100) climate under alternative GCM scenarios.
Appendix A6. Spatial distribution of predicted human-caused fire occurrence density under different GCMs scenarios.
Appendix A7. Spatial distribution of predicted lightning fire occurrence density under different GCMs scenarios.
Appendix A8. Map of relative change (percentage increase) in human-caused fire occurrence between 2100 (2081–2100) under different GCM scenarios and baseline (current fire occurrence from 1965 to 2009).
Appendix A9. Map of relative change (percentage increase) in lightning fire occurrence density between 2100 (2081–2100) under different GCM scenarios and baseline (current fire occurrence from 1965 to 2009).
Appendix A10. Pearson's chi-square test for whether human-caused fire occurrence density varied significantly among different forest types before and after 1983.
Appendix B. Model fitting algorithm for ppm() function in spatstat' package.

Please note: Wiley-Blackwell are not responsible for the content or functionality of any supporting materials supplied by the authors. Any queries (other than missing material) should be directed to the corresponding author for the article.